2014-11

Intrinsic Broadening of the Mobility Spectrum of Bulk N-Type GaAs

UTD AUTHOR(S): Massimo V. Fischetti

Jolley, G., G. A. Umana-Membreno, N. D. Akhavan, J. Antoszewski, et al. 2014. "Intrinsic broadening of the mobility spectrum of bulk n-type GaAs." New Journal of Physics 16: 113033.

New Journal of Physics
The open access journal at the forefront of physics
Deutsche Physikalische Gesellschaft DPG | IOP Institute of Physics

Intrinsic broadening of the mobility spectrum of bulk n-type GaAs

G Jolley[1], G A Umana-Membreno[1], N D Akhavan[1], J Antoszewski[1], L Faraone[1] and M V Fischetti[2]

[1] School of Electrical, Electronic and Computer Engineering, University of Western Australia, Perth, WA, 6009, Australia
[2] Department of Materials Science and Engineering, University of Texas, Dallas, Richardson, Texas 75080, USA
E-mail: gregory.jolley@uwa.edu.au

Received 21 August 2014
Accepted for publication 30 September 2014
Published 14 November 2014

New Journal of Physics **16** (2014) 113033

doi:10.1088/1367-2630/16/11/113033

Abstract

Modern devices consisting of multiple semiconductor layers often result in the population of numerous distinct carrier species. Conventional Hall measurements at a single-magnetic-field strength provide only a weighted average of the electron mobility and carrier concentration of a semiconductor structure and, therefore, are of limited use for the extraction of carrier transport information. In recent years, mobility spectrum analysis techniques, which have been developed to extract a mobility spectrum from magnetic field-dependent conductivity-tensor measurements, have been applied in the analysis of carrier conductivity mechanisms of numerous semiconductor structures and devices. Currently there is a severe lack of reported studies on theoretical calculations of the mobility distribution of semiconductor structures or devices. In addition, the majority of reports on experimental mobility spectrum analysis are of complex, multi layered structures such as type-II superlattices, and the interpretation of the mobility spectra has been difficult. Therefore, a good understanding of the mobility spectrum has yet to be developed. For example, it is often assumed that distinct peaks of a mobility spectrum result from fundamentally different conduction mechanisms such as the bulk and surface conduction of narrow-band-gap semiconductors. In this article, we present calculations of the electron mobility distribution of bulk GaAs, which predict the existence of multiple

mobility spectrum peaks that result from electron conductivity in the Γ conduction band. This report serves as an important and simple test case upon which experimentally measured mobility spectra can be compared. It also presents insight into the general nature of electron mobility distributions.

Keywords: mobility spectrum, GaAs, electron–phonon interactions

1. Introduction

Historically, the mobility of a semiconductor charge carrier is treated as a single valued function of temperature and other semiconductor parameters such as the doping density. This, in part, is due to the fact that common techniques to measure mobility are acquired at a single magnetic field strength, which results in a single value of mobility and carrier concentration. Modern semiconductor devices and structures often consist of multiple semiconductor layers, and thus contain populations of distinct carrier species caused by n- and p-doped regions, two-dimensional conduction of surface and interface layers, and thermally generated minority carriers, among other possibilities. Standard, single-magnetic-field measurements of the resistivity and Hall coefficient provide only an averaged value of the mobility and carrier concentration. Such averaged values have little physical meaning for devices where multiple carrier species, in addition to bulk majority carriers, have a strong influence on device operation. Knowledge of the mobility and carrier concentration of the individual carrier species provides valuable insight into carrier interactions and device operation, which has motivated the development of mobility spectrum analysis techniques.

Initial mobility spectrum algorithms were multicarrier fitting procedures which required prior assumptions about the number of electron and hole species and their approximate densities and mobilities. In 1987, Beck and Anderson proposed an approach known as multispectral analysis, in which they determined an envelope of the maximum conductivity as a continuous function of mobility [1]. Further developments by several research groups led to what is known as mobility spectrum analysis (MSA), in which the generated spectra are optimized to quantitatively agree with the experimentally derived magnetic field-dependent Hall and resistivity results [2–7]. Recently, MSA has been utilized to study carrier transport in a variety of semiconductor nanostructures and devices [8–27].

MSA is based upon an analysis of magnetic field-dependent conduction, which is assumed to be of the form

$$\begin{pmatrix} J_x \\ J_y \end{pmatrix} = \frac{1}{1 + \mu^2 B^2} \begin{pmatrix} ne\mu & Sne\mu^2 B \\ -Sne\mu^2 B & ne\mu \end{pmatrix} \begin{pmatrix} E_x \\ E_y \end{pmatrix}, \tag{1}$$

where n, e, μ, and B are the carrier density, the magnitude of the charge on an electron, the carrier mobility, and the magnetic field strength, respectively. S is -1 for electrons and $+1$ for holes. The magnetic field is applied in the z-direction and the current is constrained to flow in the x-and y-directions.

Within the MSA framework, the conductivity relationship is generalized to allow the conductivity-tensor components to be continuous functions of mobility,

$$\begin{pmatrix} J_x \\ J_y \end{pmatrix} = \int \mathrm{d}\mu \frac{1}{1+\mu^2 B^2} \begin{pmatrix} [n(\mu)+p(\mu)]e\mu & [p(\mu)-n(\mu)]e\mu^2 B \\ -[p(\mu)-n(\mu)]e\mu^2 B & [n(\mu)+p(\mu)]e\mu \end{pmatrix} \begin{pmatrix} E_x \\ E_y \end{pmatrix}. \quad (2)$$

MSA algorithms are analogous to a Fourier transform in the sense that conductivity is transformed from the magnetic field-strength domain to the mobility domain. To provide an understanding of mobility spectra, we present the calculation results of the mobility distribution of bulk GaAs. A complicated mobility distribution with multiple peaks resulting from electron conductivity in only the Γ conduction band is predicted. The mobility distribution is dependent on the nature of the scattering interactions, and therefore is influenced by temperature and the doping concentration. The electron kinetic energy distribution directly leads to a broadening of the mobility distribution, which is persistent over a wide temperature range for nondegenerately doped GaAs. The calculated results provide a means to evaluate and interpret experimentally derived mobility spectra.

2. Model details

To calculate the mobility distribution of n-type GaAs, the Boltzmann transport equation (BTE) is solved numerically only for conduction band electrons under the influence of an applied electric field. Consider the distribution function, $f(\mathbf{k}, t)$, which represents the probability that the electron momentum state, $|\mathbf{k}\rangle$, is occupied, and t is a time parameter. Since we are dealing with homogeneous bulk material under steady-state conditions, the distribution function has no spatial dependence.

The Boltzmann transport equation expresses the fact that under steady-state conditions, the occupation probability of any given momentum state, $|\mathbf{k}\rangle$, is time independent,

$$\frac{\mathrm{d}f(\mathbf{k}, t)}{\mathrm{d}t} = 0. \quad (3)$$

Considering the actions of the applied electric field and electron-scattering mechanisms, the steady-state condition gives

$$\frac{e}{\hbar}\mathbf{E} \cdot \nabla_{\mathbf{k}} f(\mathbf{k}, t) + \left.\frac{\partial f(\mathbf{k}, t)}{\partial t}\right|_{\mathrm{coll}} = 0, \quad (4)$$

where e is the magnitude of the electron charge, $\hbar$ is Plank's constant, and $\mathbf{E}$ is the applied electric field. The right-hand-side term of the above equation represents the rate of change of the electron momentum state occupation due to scattering events. Three scattering interactions are taken into consideration: polar optical phonons, acoustic phonons, and ionized impurities. Solving the Boltzmann transport equation provides information about how the electrons are distributed among the momentum states. From the momentum distribution, we obtained steady-state distributions such the conductivity, $\sigma(E)$, and mobility, $\mu(E)$, as a function of carrier energy, and the conductivity as a function of mobility, $\sigma(\mu)$.

The longitudinal polar optical (LO) phonon interaction takes the usual form. The rate at which an electron in an initial momentum state, $|\mathbf{k}_i\rangle$, scatters to a final state, $|\mathbf{k}_f\rangle$, is given by the following equation,

$$W\left(\mathbf{k}_i, \mathbf{k}_f\right) = \frac{e^2}{q^2}\frac{\pi}{\hbar^2}\frac{\omega_{\mathrm{LO}}(\varepsilon_s - \varepsilon_e)}{\varepsilon_e \varepsilon_s}\delta\left(E_f - E_i \pm \hbar\omega_{\mathrm{LO}}\right) \times \left(N_q + \frac{1}{2} \pm \frac{1}{2}\right)\left(1 - f\left(\mathbf{k}_f\right)\right), \tag{5}$$

where $q = |\mathbf{k}_i - \mathbf{k}_f|$ is the magnitude of the phonon wavevector, ω_{LO} is the LO phonon frequency (assumed to be dispersionless), ε_s is the static permitivity, and ε_e is the high frequency permitivity. N_q is the number of phonons occupying the mode,

$$N_q = \frac{1}{\exp\left(\hbar\omega_{LO}/k_b T\right) - 1}, \tag{6}$$

where T is the temperature and k_b is the Boltzmann constant. The upper (lower) sign of $\pm$ corresponds to emission (absorption) of phonons. The total rate at which electrons scatter from the state $\mathbf{k}_i$ is an integration over all final states,

$$\frac{\mathrm{d}}{\mathrm{d}t} f\left(\mathbf{k}_i, t\right)_{\mathrm{out}} = \int \mathrm{d}\mathbf{k}_f \frac{e^2}{q^2}\frac{\pi}{\hbar^2}\frac{\omega_{\mathrm{LO}}(\varepsilon_s - \varepsilon_e)}{\varepsilon_e \varepsilon_s}\delta\left(E_f - E_i \pm \hbar\omega_{\mathrm{LO}}\right) \times \frac{1}{(2\pi)^3}\left(N_q + \frac{1}{2} \mp \frac{1}{2}\right) f\left(\mathbf{k}_i\right)\left(1 - f\left(\mathbf{k}_f\right)\right). \tag{7}$$

The total rate at which electrons scatter into the state $\mathbf{k}_i$ is given by

$$\frac{\mathrm{d}}{\mathrm{d}t} f\left(\mathbf{k}_i, t\right)_{\mathrm{in}} = \int \mathrm{d}\mathbf{k}_f \frac{e^2}{q^2}\frac{\pi}{\hbar^2}\frac{\omega_{\mathrm{LO}}(\varepsilon_s - \varepsilon_e)}{\varepsilon_e \varepsilon_s}\delta\left(E_f - E_i \pm \hbar\omega_{\mathrm{LO}}\right) \times \frac{1}{(2\pi)^3}\left(N_q + \frac{1}{2} \pm \frac{1}{2}\right) f\left(\mathbf{k}_f\right)\left(1 - f\left(\mathbf{k}_i\right)\right). \tag{8}$$

The $(1 - f(\mathbf{k}_i))$ terms are important for degenerately doped semiconductors, but are very close to unity for the nondegenerate GaAs. Nevertheless, as considered in this work, they were included in the computational routines.

The longitudinal acoustic phonon scattering rates are evaluated by a Bardeen-Shockley deformation-potential approximation method [28], the details of which can be found in the appendix. Ionized impurity scattering is calculated within the usual Brooks-Herring approach for nondegenerate semiconductors. The scattering rate of an electron in the state $\mathbf{k}_i$ is given by

$$W\left(\mathbf{k}_i\right) = \frac{N_D}{(2\pi)^3}\int_{\mathbf{k}_f}\frac{2\pi}{\hbar}\left|\left\langle \mathbf{k}_i \left| eV(\mathbf{r}) \right| \mathbf{k}_f \right\rangle\right|^2 \left(1 - f\left(\mathbf{k}_f\right)\right)\delta\left(E_{\mathbf{k}_i} - E_{\mathbf{k}_f}\right), \tag{9}$$

where

$$V(r) = \frac{e}{4\pi\varepsilon_s r}\exp\left(-q_0 r\right). \tag{10}$$

ε_s is the static permitivity and q_0 is the screening parameter, which is dependent on the doping density, N_D,

$$q_0^2 = \frac{e^2 N_D}{\varepsilon_s k_B T}. \tag{11}$$

The band structure of the GaAs is provided as input to the scattering routines, which is calculated from an eight-band $\mathbf{k}.\mathbf{p}$ model. After the total scattering rates are calculated, including the contribution of the applied electric field, a correction is made to the electron distribution function, $f(\mathbf{k})$, based on the imbalance between the rate at which electrons leave and enter a given momentum state. The scattering rates are re-evaluated, and this process is repeated until the net scattering rate converges to zero. This fully numerical method is similar to that of Rode [29], and is commonly used for calculations involving anisotropic and inelastic scattering processes [30, 31].

For all calculations, the standard material parameters for GaAs have been provided as input, as taken from [32]. The relative static and high-frequency permitivity values are taken as 12.9 [33] and 10.89 [34], respectively.

All distributions are calculated from $f(\mathbf{k})$. The conductivity density (in the direction of the applied electric field) as a function of the electron energy is calculated by numerically evaluating the following integral

$$\sigma(E) = \frac{e}{|\mathbf{E}|}\frac{\mathbf{v}_g(k(E))}{E(k+\Delta k) - E(k)}\int_{k(E)}^{k(E)+\Delta k} \mathrm{d}k\, k^2 \times \int_0^{\pi} \mathrm{d}\theta \sin\theta\cos\theta \int_0^{2\pi} \mathrm{d}\phi\, f(k,\theta,\phi), \tag{12}$$

where θ is the angle with respect to the direction of the applied electric field, $\mathbf{v}_g = \partial\omega/\partial|\mathbf{k}|$ is the electron group velocity, and $|\mathbf{E}|$ is the magnitude of the applied electric field. $\omega = E(|\mathbf{k}|)/\hbar$ is the angular frequency of the electronic state and the electron group velocity, $\mathbf{v}_g$, is in the direction of $\mathbf{k}$.

The mobility as a function of electron energy is obtained from the conductivity density and the differential carrier density.

$$\mu(E) = \frac{\sigma(E)\Delta E(\Delta k)}{e} \Big/ \int_{k(E)}^{k(E)+\Delta k} \mathrm{d}k\, k^2 \times \int_0^{\pi} \mathrm{d}\theta \sin\theta \int_0^{2\pi} \mathrm{d}\phi\, f(k,\theta,\phi) \tag{13}$$

$\mu(E)$ and $\sigma(E)$ allow for the construction of the mobility distribution function, $\sigma(\mu)$, which indicates the contribution to the conductivity of carriers with a particular mobility. A mobility slice of finite width is chosen, $(\mu \to \mu + \Delta\mu)$, and the energy ranges, $E_1 \to E_1 + \Delta E_1, \cdots, E_n \to E_n + \Delta E_n$, for which the mobility distribution $(\mu(E))$ falls within the mobility of the chosen slice are determined. The conductivity is then determined by,

$$\sigma(\mu \to \mu + \Delta\mu) = \int_{E_1}^{E_1+\Delta E_1} dE\, \sigma(E) + \cdots + \int_{E_n}^{E_n+\Delta E_n} dE\, \sigma(E). \tag{14}$$

Modern mobility spectrum algorithms typically split the mobility domain into 20 slices per decade [4], and therefore we have done the same for the computation results presented in this paper.

3. Results and discussion

The computational methods described have been applied to bulk GaAs for various temperatures and a doping concentration of 1×10^{16} cm^{-3} and 1×10^{17} cm^{-3}. Figures 1 and 2 show the

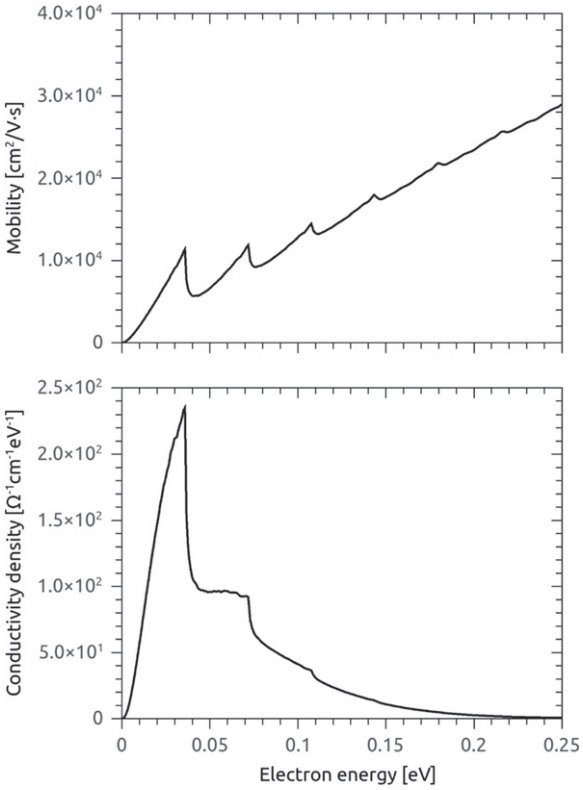

Figure 1. Calculated conductivity density as a function of electron energy, and calcuted electron mobility as a function of electron energy for bulk GaAs at a temperature of 300 K and an electron concentration of 1×10^{16} cm^{-3}. The average electron mobility is 6820 cm^2(Vs)$^{-1}$.

computational results for a temperature of 300 K and an electron concentration of 1×10^{16} cm^{-3}. Figure 1 shows the electron mobility and conductivity density as a function of electron kinetic energy, and figure 2 is a plot of the resultant mobility distribution. The calculated average mobility is 6820 cm^2(Vs)$^{-1}$, which is in agreement with experimentally determined values of the drift mobility for room-temperature bulk GaAs with a carrier concentration of 1×10^{16} cm^{-3}. An interesting feature of the $\mu(E)$ and $\sigma(E)$ plots is their sudden reductions in magnitude, which occur at integer multiples of the LO phonon energy (36 meV). A reduction of mobility and conductivity is expected at the LO phonon energy point, since LO phonon scattering is the dominant scattering mechanism for GaAs at room temperature and $E = 36$ meV is the threshold for LO phonon emission, which results in a dramatic increase in the electron scattering rate. The subsequent reductions at larger energies are a result of the tendency for LO phonon scattering to occur for smaller phonon wavevectors. Consider the change in the distribution function due to the applied electric field,

$$f(k, \theta, \phi) = f^0(k, \theta, \phi) + \Delta f(k, \theta, \phi), \tag{15}$$

where $f^0(k, \theta, \phi)$ is the electron distribution under thermal equilibrium conditions and $\Delta f(k, \theta, \phi)$ is the change in distribution as a result of the applied electric field. For a given electron energy, E, $\Delta f(k(E), \theta, \phi)$ tends to obtain a maximal value in the direction opposite to the applied field ($\theta = \pi$), and the tendency of LO phonon absorption to occur in the direction of the electron wavevector influences the value of $\Delta f(k(E + E_{LO}), \pi, \phi)$. Essentially, an increase

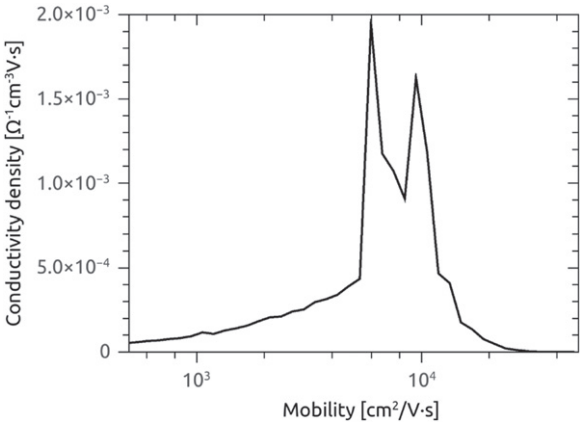

Figure 2. The mobility distribution, $\sigma(\mu)$, of GaAs at a temperature of 300 K and an electron concentration of 1×10^{16} cm^{-3}.

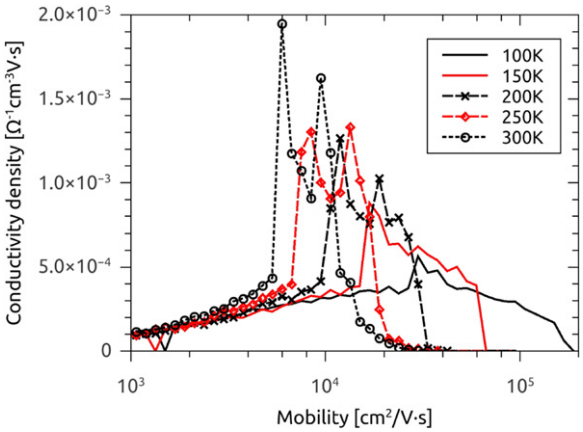

Figure 3. The mobility distribution, $\sigma(\mu)$, of GaAs for various temperatures and an electron concentration of 1×10^{16} cm^{-3}. The calculated average mobilities are 3.0×10^4, 1.9×10^4, 1.2×10^4, 8.8×10^3, and 6.8×10^3 cm^2(Vs)$^{-1}$ for temperatures of 100, 150, 200, 250, and 300 K, respectively.

of $\Delta f(k(E), \pi, \phi)$ causes an increase of $\Delta f(k(E + E_{LO}), \pi, \phi)$ due to preferential forward scattering. Likewise, the sudden reduction of $\Delta f(k(E = E_{LO}), \pi, \phi)$ causes a reduction of $\Delta f(k(E + E_{LO}), \pi, \phi)$, resulting in the multiple dips featured in $\mu(E)$. The multiple dips and troughs of the mobility function, $\mu(E)$, show up as a series of peaks in the mobility distribution, $\sigma(\mu)$.

Plots of $\sigma(\mu)$ for a range of temperatures are shown in figure 3. Decreasing temperature leads to a reduction in magnitude of the $\sigma(\mu)$ peaks at higher mobility. This is a consequence of the fact that fewer electrons have enough thermal energy to populate states with an energy greater than the LO phonon energy. For a temperature of 100 K, the $\sigma(\mu)$ distribution is very broad and only a single peak exists. Some general observations can be made regarding the nature of the calculated mobility distribution. First, the mobility distributions are rather broad, and second, the subsequent peaks of the mobility distribution occur at larger mobility. The broad, calculated mobility distribution is a result of the approximate square root dependence of the GaAs, electron group velocity on the electron energy. The group velocity term in

equation (12), together with equation (13), results in a large mobility spread with electron kinetic energy. This directly leads to the broad mobility distribution, particularly at low temperatures, such that there are no polar optical phonon-related peaks. For semiconductors that are heavily doped, the mobility distribution may become narrow at low temperatures, since carrier interactions and transport predominantly occur at the Fermi level. However, for the results presented here, at a temperature of 100 K and an electron concentration of 1×10^{16} cm^{-3}, the Fermi level is 18 meV below the conduction band edge, and therefore conduction occurs over a large relative electron energy range. As shown in figure 1, the mobility increases with each polar optical phonon emission-related dip. Therefore, each subsequent peak of the mobility distributions occurs at larger mobility.

The nature of the scattering interactions, and therefore of the electron concentration, has an impact on the mobility distribution. Figures 4 and 5 show results for a temperature of 300 K and a carrier concentration of 1×10^{17} cm^{-3}. An increase of the carrier concentration results in a relatively larger ionized impurity scattering rate, which tends to mask the effects of the LO phonon scattering. This results in shallower dips in the mobility function, $\mu(E)$, and the second peak of the $\sigma(\mu)$ distribution has a reduced magnitude relative to the first peak. A mobility distribution, $\sigma(\mu)$, that features more that a single peak is expected to occur for a wide variety of semiconductor materials and structures, provided that the LO phonon scattering dominates the total carrier scattering rate. These conditions are likely to hold for polar semiconductors with a low to moderate concentration of impurity atoms at a temperature greater than about 200 K. For structures such as superlattices with mobilities that are limited by interface roughness scattering, LO phonon interactions are less likely to have a significant influence on the qualitative features of the mobility distributions.

The development of mobility spectrum algorithms initially considered populations of distinct carrier species, and assumptions had to be made regarding the number of species present. Modern algorithms consider a continuum of carrier mobility, and therefore no prior assumptions need to be made regarding the number of carrier species that are present in a semiconductor sample under consideration. However, there is a tendency to assume that the individual peaks of a mobility spectrum originate from distinctly different carrier conduction mechanisms such as the surface and bulk conduction of narrow-band-gap semiconductors. Designating carriers into distinct species can be a completely inadequate description, since carriers generally occupy a continuum of states with a coupling between states that can vary greatly depending on the available phonon modes and the overlap of wavefunctions. For example, the bulk and surface carrier conduction of a narrow-band-gap semiconductor occur in spatially separate regions, and therefore the coupling of carriers between these two conduction mechanisms is minimal, whereas the carriers occupying the ground and excited state subbands of a quantum well superlattice [35] are tightly coupled by phonon transitions. Given the thermal energy distribution of carriers, it is evident that within a mobility spectrum approach, carriers should be considered to occupy a continuum of states, which can have important consequences on the mobility spectrum.

An exact solution of the BTE can be computationally expensive, and other methods of determining carrier mobility are common in the literature. A particularly popular method for calculating mobility is a momentum relaxation approach of the following form,

$$\mu = \frac{e}{m^*} \frac{\langle E\tau \rangle}{\langle E \rangle} \tag{16}$$

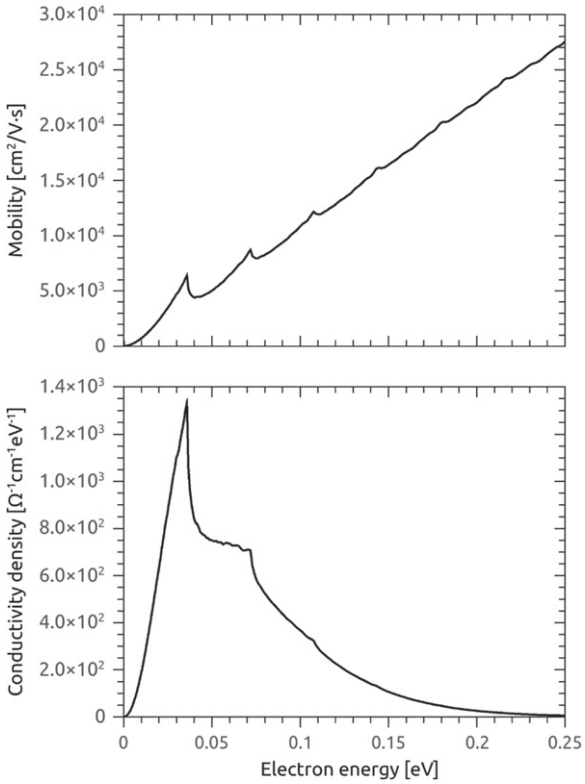

Figure 4. Calculated conductivity density as a function of electron energy, and calculated electron mobility as a function of electron energy for bulk GaAs at a temperature of 300 K and an electron concentration of $1 \times 10^{17}\text{cm}^{-3}$. The average electron mobility is $4770\,\text{cm}^2(\text{Vs})^{-1}$.

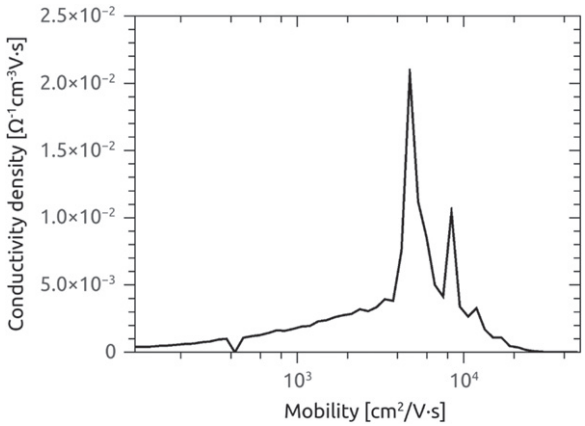

Figure 5. The mobility distribution, $\sigma(\mu)$, of GaAs at a temperature of 300 K and an electron concentration of 1×10^{17} cm^{-3}.

where E is the electron kinetic energy and τ is the carrier momentum relaxation lifetime derived from scattering rates of the following form,

$$\frac{1}{\tau} = \int \mathrm{d}\mathbf{k}_f \, W\left(\mathbf{k}_i, \mathbf{k}_f\right)\left(1 - \frac{\left|\mathbf{k}_f\right|}{\left|\mathbf{k}_i\right|}\cos\theta_{if}\right) \tag{17}$$

where $W(\mathbf{k}_i, \mathbf{k}_f)$ is the scattering rate from state $\mathbf{k}_i$ to $\mathbf{k}_f$ and θ_{if} is the scattering angle between $\mathbf{k}_i$ and $\mathbf{k}_f$.

An energy dependence can be introduced into the mobility,

$$\mu(E) = \frac{e}{m^*}\frac{E\tau(E)}{\langle E\rangle}, \tag{18}$$

An energy-dependent conductivity density can also be obtained by the following description,

$$\sigma(E) = e\mu(E)n_c(E), \tag{19}$$

where $n_c(E)$ is the carrier density per unit of carrier energy. To demonstrate the influence that the common momentum relaxation approach described above has on the calculated mobility distribution, calculations have been performed for various temperatures and an electron concentration of 1×10^{16} cm^{-3}. The momentum relaxation approach described above cannot obtain mobility or conductivity functions with the level of detail of more complete solutions of the BTE. This can be seen by the results shown in figure 6. The corresponding mobility distributions shown in figure 7 contain single mobility peaks that result from the plateau of the mobility as a function of energy, for energies just beyond the LO phonon energy.

Reports on MSA measurements cover a wide range of semiconductor materials and structures, the majority of which are complex multilayered structures, so there are few reports that the work presented in this paper can be directly compared to. However, it can be concluded that MSA measurements tend to return mobility spectra with conductivity that occurs over a considerably narrower mobility range. See, for example, the MSA reports by Brown *et al* of single-layer n-type HgCdTe and InP epi layers [27], Hudait *et al* on $InAs_1P_{1-x}$ [36], and Umana-Membreno *et al* on LPE-grown Hg_xCd_xTe layers [26].

There is no compelling evidence of multiple MSA peaks due to a polar optical phonon interaction in the literature. Hudait *et al* [36] performed an analysis on 1.5 μm thick epilayers of $InAs_xP_{1-x}$, Si-doped to a concentration of 2×10^{16} cm^{-2}, using the quantitative MSA algorithm, which indicates the presence of multiple peaks in the electron mobility spectrum due to conduction within the epilayers. An earlier work by Achard *et al* [10], which studied the mobility spectrum of InP epilayers using an older mobility spectrum algorithm, reported only a single mobility peak at higher temperatures. Acar *et al* [25] reported on the measured mobility spectrum of bulk GaSb, indicating the possibility that LO phonon scattering resulted in two peaks in the mobility spectrum. For higher temperatures, the mobility spectrum splits into two peaks that are closely spaced in mobility. The occurrence of the second peak is attributed by Acar *et al* to the population of the L conduction band with electrons, due to its small energy separation (≈ 75 meV) from the Γ band. Considering that the ratio of electron mobilities in the L and Γ bands, μ_L/μ_Γ, is about 0.1 [37], it is possible that the L band conduction occurs at a lower mobility range that is outside of the plots presented in [25], and that both peaks result from conduction in only the Γ band. A particularly interesting report published recently by Brown *et al* [27] studied the mobility spectrum of nondegenerate molecular beam epitaxy-

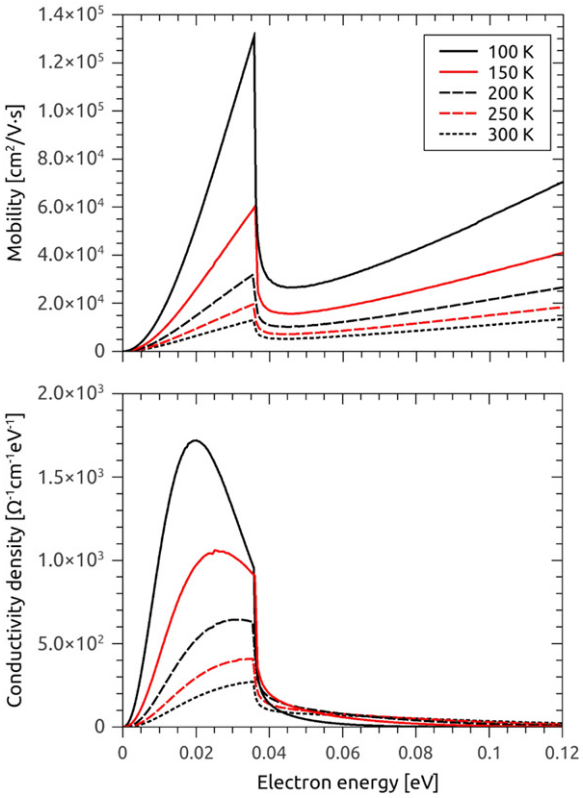

Figure 6. Calculated conductivity density and mobility as a function of electron energy for bulk GaAs at various temperatures and an electron concentration of $1 \times 10^{16}\text{cm}^{-3}$. These results are calculated using the momentum relaxation approximation.

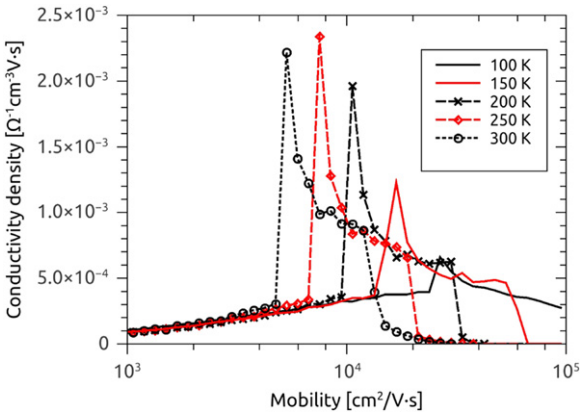

Figure 7. The mobility distribution, $\sigma(\mu)$, of GaAs for various temperatures and an electron concentration of 1×10^{16} cm^{-3}, as derived from the momentum relaxation approximation.

grown n-type $Hg_{1-x}Cd_xTe$ epilayers. The mobility spectrum of these epilayers exhibited a double peak for temperatures greater than about 150–200 K. These two peaks are attributed to conduction in regions of different Hg content, and hence different mobility. This view is supported by measurements of the composition profiles of the $Hg_{1-x}Cd_xTe$ layers, which show a dramatic increase of the cadmium fraction for regions towards the epilayer/substrate interface. However, the evolution of the lower mobility peak, which becomes evident for temperatures greater than 150 K, is closely separated in mobility from the higher mobility peak (within a factor of two), which is qualitatively very similar to the GaA results calculated in this work. Therefore, it seems possible that the double peak is due to the inherent mobility spectrum of $Hg_{1-x}Cd_xTe$. This is supported by the fact that the mobility of mercury cadmium telluride is strongly dependent on the cadmium content, and all three $Hg_{1-x}Cd_xTe$ epilayer samples grown on different substrates display similar mobility spectra. Similarly, Umana-Membreno *et al* [26] studied liquid-phase epitaxy-grown HgCdTe epilayers of 20 μm thickness. The mobility spectra displayed closely spaced double peaks, which are attributed to electron conduction in regions of different cadmium content. Given the computational results presented in this work, predicting that multiple peaks of a mobility spectrum can naturally arise from carrier transport in bulk material due to electron-polar optical phonon scattering, the assumption that different peaks of a mobility spectrum are due to different carrier transport mechanisms may not be valid.

It is not a forgone conclusion that the results presented here would match those of the experiment. A central question is whether the various nonideal aspects of experimental Hall measurements should be expected to substantially influence the derived spectra. Particular concerns include effects such as a nonideal Hall bar or van der Pauw geometry, lateral inhomogeneities of the material, contact resistance, finite magnetic field range, possible effects of the Hall factor, and the range of validity of the conductivity-tensor components given by equation (2). Further work must be done on understanding the limitations of MSA and the effects of nonideal experimental influences on the derived mobility spectrum.

4. Conclusions

We have presented calculations of the electron mobility distribution of bulk GaAs that reveal some interesting features of the mobility distribution due to conduction within the Γ band. We found that the mobility distribution of GaAs is considerably complex, with a shape that depends on the nature of the scattering interactions. We predicted that under conditions where the optical phonon interaction is the dominant scattering mechanism, multiple peaks are present in the $\sigma(\mu)$ spectrum. This suggests that the interpretation of experimental quantitative mobility spectrum analysis requires careful consideration and, in particular, the assignment of individual peaks of the mobility spectrum to different conduction mechanisms may not be valid in some situations. In addition, the calculated conductivity occurred over a broad mobility range, which is a consequence of the thermal energy distribution of electrons.

Acknowledgments

The authors wish to thank the Australian Research Council (ARC) for financially supporting this work (ARC grant numbers FS110200022 and DP120104835).

Appendix A. Acoustic phonon scattering rates

The classical continuum elastic acoustic modes are calculated, from which the hydrostatic strain is determined for an acoustic mode equal to the phonon energy, $E = \hbar\omega$. Acoustic mode solutions are assumed to take the following form,

$$\mathbf{p}(\mathbf{r}, t) = \frac{\mathbf{a}}{2}(\exp[\mathrm{i}(\mathbf{q} \cdot \mathbf{r} - \omega t)] + \exp[\mathrm{i}(-\mathbf{q} \cdot \mathbf{r} + \omega t)]), \tag{A.1}$$

where $\mathbf{p}(\mathbf{r}, t)$ is the atomic displacement function of the acoustic mode, $\mathbf{a}$ is an atomic displacement vector, $\mathbf{q}$ is the acoustic wavevector, and ω is the frequency of the acoustic mode. Putting the solution form into the equations of motion results in a set of equations,

$$\begin{aligned}
\rho\omega^2 a_1 &= C_{11}a_1q_1^2 + (C_{12} + C_{44})\left(a_2q_1q_2 + a_3q_1q_3\right) + C_{44}a_1\left(q_2^2 + q_3^2\right)\\
\rho\omega^2 a_2 &= C_{11}a_2q_2^2 + (C_{12} + C_{44})\left(a_1q_1q_2 + a_3q_2q_3\right) + C_{44}a_2\left(q_1^2 + q_3^2\right)\\
\rho\omega^2 a_3 &= C_{11}a_3q_3^2 + (C_{12} + C_{44})\left(a_1q_1q_3 + a_2q_2q_3\right) + C_{44}a_3\left(q_1^2 + q_2^2\right)
\end{aligned} \tag{A.2}$$

where the C coefficients are the elastic constants of the GaAs and ρ is the mass density of the GaAs. The displacements are found by solving an eigen equation of the form,

$$\mathbf{Ra} = \rho\omega^2\mathbf{a}, \tag{A.3}$$

where $\mathbf{R}$ is the following matrix

$$\begin{bmatrix}
C_{11}q_1^2 + C_{44}\left(q_2^2 + q_3^2\right) & (C_{12} + C_{44})q_1q_2 & (C_{12} + C_{44})q_1q_3\\
(C_{12} + C_{44})q_1q_2 & C_{11}q_2^2 + C_{44}\left(q_1^2 + q_3^2\right) & (C_{12} + C_{44})q_2q_3\\
(C_{12} + C_{44})q_1q_3 & (C_{12} + C_{44})q_2q_3 & C_{11}q_3^2 + C_{44}\left(q_1^2 + q_2^2\right)
\end{bmatrix} \tag{A.4}$$

There are three solutions of the eigen equation, and of these solutions, only the longitudinal mode is of interest. The magnitudes of the atomic displacements are set such that the elastic energy is equal to the phonon energy,

$$W = \hbar\omega = \frac{1}{2}\varepsilon\,[E]\,\varepsilon, \tag{A.5}$$

where $[E]$ is the elastic stiffness matrix of the GaAs and the strain components are given by the usual terms

$$e_{xx} = \frac{\partial u}{\partial x} = a_1q_1; \quad e_{yy} = a_2q_2; \quad e_{zz} = a_3q_3; \quad e_{xy} = \frac{\partial u}{\partial y} + \frac{\partial v}{\partial x} = a_1q_2 + a_2q_1; \text{ etc.} \tag{A.6}$$

The scattering perturbation is

$$\mathbf{H}'_q(\mathbf{r}, \mathbf{t}) = a_c\varepsilon_{\mathrm{hyd}}(\mathbf{q})\frac{1}{2}[\exp(\mathrm{i}(\mathbf{r} \cdot \mathbf{q}) - \omega t) + \exp(-\mathrm{i}(\mathbf{r} \cdot \mathbf{q}) + \omega t)], \tag{A.7}$$

where a_c and $\varepsilon_{\mathrm{hyd}}$ are the conduction band deformation parameter and the hydrostatic strain, respectively. The commonly used GaAs, conduction band deformation parameter of 7.17 eV [32] is used in this work. Using a similar method to that described above for LO phonons, the total scattering rates are calculated for each $\mathbf{k}_i$ momentum state.

References

[1] Beck W A and Anderson J R 1987 Determination of electrical transport properties using a novel magnetic field-dependent Hall technique *J. Appl. Phys.* **62** 541

[2] Meyer J R, Hoffman C A, Bartoli F J, Arnold D J, Sivananthan S and Faurie J P 1993 Methods for magnetotransport characterization of IR detector materials *Semicond. Sci. Technol.* **8** 805

[3] Dziuba Z and Górska M 1992 Analysis of the electrical conduction using an iterative method *J. Phys. III France* **2** 99

[4] Vurgaftman I, Meyer J R, Hoffman C A, Redfern D, Antoszewski J, Faraone L and Lindemuth J R 1998 Improved quantitative mobility spectrum analysis for Hall characterization *J. Appl. Phys.* **84** 4966

[5] Chrastina D, Hague J P and Leadley D R 2003 Application of Bryan's algorithm to the mobility spectrum analysis of semiconductor devices *J. Appl. Phys.* **94** 6583

[6] Kiatgamolchai S, Myronov M, Mironov O A, Kantser V G, Parker E H C and Whall T E 2002 Mobility spectrum computational analysis using a maximum entropy approach *Phys. Rev.* E **66** 036705

[7] Rothman J, Meilhan J, Perrais G, Bellie J P and Gravrand O 2006 Maximum entropy mobility spectrum analysis of HgCdTe heterostructures *J. Electron. Mater.* **35** 1174

[8] Dziuba Z 1996 Analysis of electrical conduction in epitaxial layer structures using the mobility spectrum technique *Phys. Status Solidi* A **153** 445

[9] Panaevy I A, Studenikiny S A, Tkachenkoy V A, Tkachenkoy O A, Heremansz J P, Partinz D L, Morelliz D T and Thrush C M 1996 An investigation of the multicarrier transport properties of δ-doped InSb at high temperatures using a mobility spectrum technique *Semicond. Sci. Technol.* **11** 1857

[10] Achard J, Guillot C, Barbarin F, Dugay M and Goumet E 1999 Electrical characterization of InP epitaxial layers using mobility spectrum technique *Appl. Surf. Sci.* **142** 455

[11] Lin Y, Arehart A R, Carlin A M and Ringel S A 2008 'Separation of bulk and surface electron transport in metamorphic InAs layers using quantitative mobility spectrum analysis *Appl. Phys. Lett.* **93** 62109

[12] Lisesivdin S B, Yildiz A, Acar S, Kasap M, Ozcelik S and Ozbay E 2007 Electronic transport characterization of AlGaN/GaN heterostructures using quantitative mobility spectrum analysis *Appl. Phys. Lett.* **91** 102113

[13] Reginski K, Marczewski J, Dziuba Z and Grodzicka E 1997 Mobility spectrum approach in the analysis of the electrical conduction of a GaAs layer grown by molecular beam epitaxy *J. Appl. Phys.* **82** 6102

[14] Umana-Membreno G A, Antoszewski J and Faraone L 2013 Mobility spectrum analysis of carrier transport at insulator/semiconductor interfaces *Microelectron. Eng.* **109** 232

[15] Tanaka T, Tsuchiya G, Hoshi Y, Sawano K, Shiraki Y and Itoh K M 2012 Experimental and theoretical analysis of the temperature dependence of the two-dimensional electron mobility in a strained Si quantum well *J. Appl. Phys.* **111** 073715

[16] Antoszewski J, Faraone L, Vurgaftman I, Meyer J R and Hoffman C A 2004 Application of quantitative mobility-spectrum analysis to multilayer HgCdTe structures *J. Electron. Mater.* **33** 673

[17] Antoszewski J and Faraone L 2004 Quantitative mobility spectrum analysis (QMSA) in multi-layer semiconductor structures *Opto-Electron. Rev.* **12** 347

[18] Antoszewski J, Umana-Membreno G A and Faraone L 2012 High-resolution mobility spectrum analysis of multicarrier transport in advanced infrared materials *J. Electron. Mater.* **41** 2816

[19] Fehlberg T B, Umana-Membreno G A, Gallinat C S, Koblmüller G, Bernardis S, Nener B D, Parish G and Speck J S 2007 Characterisation of multiple carrier transport in indium nitride grown by molecular beam epitaxy *Phys. Status Solidi* A **4** 2423

[20] Tasli P, Lisesivdin S B, Yildiz A, Kasap1 M, Arslan E, Özcelik S and Ozbay E 2010 Well parameters of two-dimensional electron gas in $Al_{0.88}In_{0.12}N$/AlN/GaN/AlN heterostructures grown by MOCVD *Cryst. Res. Technol.* **45** 133

[21] Swartz C H, Tompkins R P, Giles N C, Myers T H, Lu H, Schaff W J and Eastman L F 2004 Investigation of multiple carrier effects in InN epilayers using variable magnetic field Hall measurements *J. Cryst. Growth* **269** 29

[22] Myronov M, Irisawa T, Mironov O A, Koh S, Shiraki Y, Whall T E and Parker E H C Extremely high room-temperature two-dimensional hole gas mobility in Ge/$Si_{0.33}Ge_{0.67}$/Si(001) p-type modulation-doped heterostructures *Appl. Phys. Lett.* **80** 3117

[23] Rawdanowicz T A, Iyer S, Mitchel W C, Saxler A and Elhamri S 2002 Electronic properties of heteroepitaxial undoped and n-InSb epilayers using SnTe source by molecular beam epitaxy *J. Appl. Phys.* **92** 296

[24] Umana-Membreno G A, Klein B, Kala H, Antoszewski J, Gautam N, Kutty M N, Plis E, Krishna S and Faraone L 2012 Vertical minority carrier electron transport in p-type InAs/GaSb type-II superlattices *Appl. Phys. Lett.* **101** 253515

[25] Acar S, Kasap M, Isik B Y, Ozcelik S, Tugluoglu N and Karadeniz S 2005 Quantitative mobility spectrum analysis for determination of electron and magneto transport properties of Te-doped GaSb *Chin. Phys. Lett.* **22** 2363

[26] Umana-Membreno G A, Antoszewski J, Faraone L, Smith E P G, Venzor G M, Johnson S M and Phillips V 2010 Investigation of multicarrier transport in LPE-grown $Hg_{1-x}Cd_xTe$ layers *J. Electron. Mater.* **39** 1023

[27] Brown A E, Jaime-Vasquez M, Almeida L A, Arias J, Lennon C M, Jacobs R N, Pellegrino J and Sivananthan S 2013 Variable-field Hall measurement and transport in LW single-layer n-type MBE $Hg_{1-x}Cd_xTe$ *J. Electron. Mater.* **42** 3224

[28] Bardeen J and Shockley W 1950 Deformation potentials and mobilities in non-polar crystals *Phys. Rev.* **80** 72

[29] Rode D L 1970 Electron mobility in direct-gap polar semiconductors *Phys. Rev.* B **2** 1012

[30] Fletcher K and Butcher P N 1972 An exact solution of the linearized Boltzmann equation with applications to the Hall mobility and Hall factor of n-GaAs *J. Phys. C: Solid State Phys.* **5** 212

[31] Ridley B K 1998 Polar-optical-phonon and electron-electron scattering in large-bandgap semiconductors *J. Phys.: Condens. Matter* **10** 6717

[32] Vurgaftman I, Meyer J R and Ram-Mohan L R 2001 Band parameters for IIIV compound semiconductors and their alloys *J. Appl. Phys.* **89** 5815

[33] Neidert R E 1980 Dielectric constant of semi-insulating gallium arsenide *Electron. Lett.* **16** 244

[34] Samara G A 1983 Temperature and pressure dependences of the dielectric constants of semiconductors *Phys. Rev.* B **27** 3494

[35] Ahn I-H, Song G H and Jho Y-D 2010 Separating the contribution of mobility among different quantum well subbands *Japan. J. Appl. Phys.* **49** 14102

[36] Hudait M K, Lin Y, Sinha P M, Lindemuth J R and Ringel S A 2006 Carrier compensation and scattering mechanisms in Si-doped $InAs_yP_{1y}$ layers grown on InP substrates using intermediate $InAs_yP_{1y}$ step-graded buffers *J. Appl. Phys.* **100** 063705

[37] Cederberg J G and Biefeld R M 2004 The growth of n-type GaSb by metal-organic chemical vapour deposition: effects of two-band conduction on carrier concentrations and donor activation *Semicond. Sci. Technol.* **19** 953